Structural Durability & Health Monitoring

Tech Science Press

https://doi.org/10.32604/sdhm.2026.077926

ARTICLE

Tilt Measurement Method of Wooden Columns in Traditional Timber Buildings Based on Adaptive RANSAC and PCA Method

Minyan Zhan[1], Wei Yang[2,3], Minghao Wu[4,*], Hsin-Yi Wang[5] and Yu-Hsien Ho[5]

[1]Urban and Rural Architecture School, Minxi Vocational & Technical College, Longyan, China
[2]Fujian Academy of Building Research Co., Ltd., Fuzhou, China
[3]Fujian Provincial Key Laboratory of Green Building Technology, Fuzhou, China
[4]College of Civil Engineering, Fujian University of Technology, Fuzhou, China
[5]Department of Civil Engineering and Geomatics, Cheng Shiu University, Kaohsiung, Taiwan

*Corresponding Author: Minghao Wu. Email: 19882326@fjut.edu.cn

Received: 19 December 2025; Accepted: 13 February 2026; Published: 18 May 2026

ABSTRACT: The inclination of wooden columns is a key indicator for evaluating the structural safety of traditional timber buildings in China. However, accurate measurement is challenging because these columns typically exhibit natural tapering, with diameters decreasing from the base to the top, and surface irregularities such as artificial cuts, cracks, and knots. Both the intrinsic geometric characteristics and surface defects reduce the precision of coordinate acquisition and the reliability of inclination estimation. To overcome these limitations, this study proposes a novel inclination measurement method for wooden columns in traditional timber buildings based on multi-section measurement and spatial line fitting. An adaptive random sample consensus algorithm is employed to effectively remove outliers induced by surface damage and measurement noise. Subsequently, principal component analysis is used to fit a three-dimensional spatial line through the center points of multiple cross-sections, enabling accurate computation of the inclination angle while accounting for structural imperfections. Moreover, the effects of damage defects, the number of measuring points, the measurement range, and the number of selected cross-sections on measurement accuracy are systematically investigated through statistical analysis, and corresponding recommended values for engineering practice are provided. The proposed method offers an efficient and reliable solution for inclination measurement, supporting the inspection and structural safety assessment of traditional timber columns.

KEYWORDS: Traditional timber building; inclination measurement of wooden column; adaptive random sample consensus algorithm; principal component analysis

1 Introduction

The inclined deformation of wooden columns is a key indicator for evaluating the damage state and structural reliability of traditional timber buildings [1–3]. During natural growth, trees develop a characteristic taper, with the diameter gradually decreasing from the base to the top. When such trees are processed into structural columns, craftsmen typically preserve this tapered geometry [4]. Although tapering contributes to the overall stability of timber columns, it significantly complicates the accurate measurement of column inclination in engineering practice. At present, inspection agencies commonly employ total stations or plumb-line methods to estimate inclination by measuring the distance difference between the upper and lower portions of a column along the same reference direction. However, in field applications, it is difficult to determine whether the observed distance difference originates from the actual tilt of the column

or from its inherent tapered geometry, as illustrated in Fig. 1. This ambiguity can lead to systematic errors in inclination assessment.

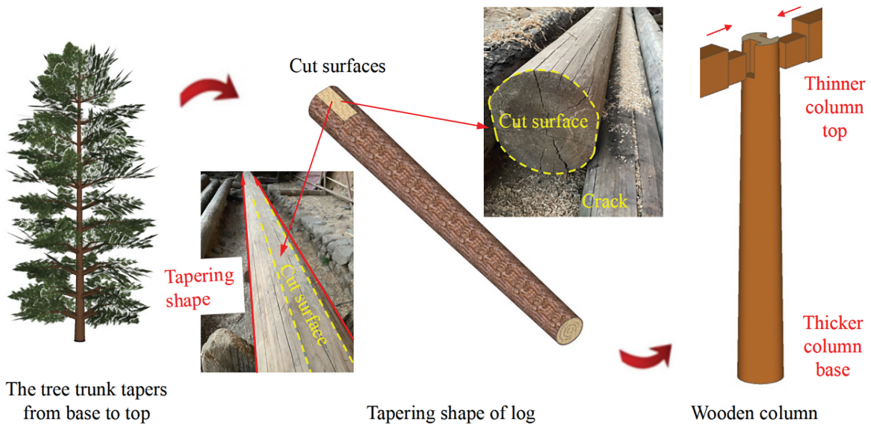

Figure 1: Diagram of tapered feature, machined cutting surfaces and defects of wooden column.

Current structural deformation measurement techniques can generally be classified into contact and non-contact methods. Early investigations of traditional timber buildings primarily relied on contact devices such as displacement gauges and inclinometers. Subsequently, several scholars proposed deformation monitoring approaches based on distributed optical fiber sensing [4,5]. Although effective, these systems require high equipment and maintenance costs and can capture only the magnitude of deformation variation, rather than the absolute deformation state of the structure. Non-contact techniques usually obtain structural deformation information by periodically collecting image or point cloud data. For example, some studies employ three-dimensional (3D) laser scanning to acquire full-surface coordinate data of wooden columns [6–8], and then estimate the central axis vector using fitting algorithms. However, this approach places stringent demands on data completeness. When point clouds in certain regions are missing due to obstructions such as walls, the fitting accuracy can deteriorate significantly or even result in failure. Methods based on Unmanned Aerial Vehicle (UAV) image recognition have also been applied to deformation monitoring of traditional buildings [9–11]. Their accuracy depends heavily on the performance of oblique photogrammetry and image recognition algorithms, and they are difficult to implement in confined indoor environments where walls block the field of view. In addition, both laser scanning and image-based techniques require substantial hardware investment and are time-consuming. Alternatively, some researchers measure coordinates of points on cross-sections at different heights of a structure, determine the sectional centers using the least squares method (LSM) [12,13], and then compute column inclination by evaluating the offset between the upper and lower centers. This technique involves simple field operations and data processing, can be implemented using only a total station, and has therefore been widely adopted for inclination measurement of structures such as ancient masonry pagodas and chimneys. Nevertheless, applying this method to traditional timber buildings still faces several technical challenges. Timber surfaces often contain irregular processing cuts, and the material is prone to damage such as cracks and wrinkles caused by drying shrinkage [14–16] (as shown in Fig. 1), which makes it difficult to form an ideal circular cross-section [17]. If measurement points fall within these defective regions, the fitting accuracy of LSM can be severely compromised. Moreover, during on-site measurements, the large distance between operators and the target columns makes it difficult to judge whether points lie on damaged or cut areas, rendering such errors largely unavoidable. In addition, wooden columns in traditional buildings are frequently connected to or partially concealed by walls, which obstruct the line of sight and lead to incomplete surface coordinate acquisition, further degrading measurement

precision. At present, the selection of the number of measurement points in field practice relies mainly on operator experience, and scientific, unified guidelines are still lacking.

Accordingly, this paper proposes an inclination measurement method for wooden columns in traditional buildings that integrates an adaptive Random Sample Consensus (RANSAC) algorithm [18,19] with principal component analysis (PCA) [20,21]. The adaptive RANSAC procedure is first employed to detect and remove abnormal measurement points located in defective or damaged regions of the column surface. Subsequently, PCA is used to spatially fit the effective centers of multiple cross-sections and determine the direction vector of the column axis, thereby enabling accurate estimation of column inclination. In addition, error statistical analysis is conducted to investigate how the number of measurement points and the measurement range required by the proposed method influence measurement accuracy. Finally, the effectiveness and practical applicability of the method are validated through a real-world case study involving an in-service traditional timber building.

2 Methods

2.1 Solving Traditional Wooden Column Cross-Section Center Coordinates via RANSAC

2.1.1 The RANSAC Algorithm

The RANSAC algorithm is adopted to identify and eliminate measurement points located in damaged, defective, or cut regions of wooden columns [22–24]. Suppose that the number of measured points on a given cross-section of a wooden column is $\boldsymbol{N}$, and the coordinates of each point in the sectional plane are denoted as $P_i(x_i,y_i)$, where $i = 1, 2, \ldots, n$. In each iteration (i.e., one fitting process), three points are randomly selected from the complete set of measured points to determine the center of the fitted circle. Let the total number of iterations be k. For the j-th iteration, three points P1, P2 and P3 are randomly chosen, with coordinates P1(x_1,y_1), P2(x_2,y_2) and P3(x_3,y_3) respectively. The circle center coordinates are then calculated using the following equations:

$$(x_{ic} - x_1)^2 + (y_{ic} - y_1)^2 = {r_i}^2 \tag{1}$$

$$(x_{ic} - x_2)^2 + (y_{ic} - y_2)^2 = {r_i}^2 \tag{2}$$

$$(x_{ic} - x_3)^2 + (y_{ic} - y_3)^2 = {r_i}^2 \tag{3}$$

where, x_{ic} and y_{ic} denote the circle center coordinates obtained in the i-th iteration, which are solved using Eqs. (1)–(3). For the remaining measurement points P_4~P_N in the dataset, their distances to the fitted circle center are calculated using Eq. (4), where "d" represents the distance from a given measurement point to the circle center. A threshold value [d] is defined such that if $d_i \geq [d]$, the point is classified as an outlier; otherwise, it is considered an inlier.

$$d_i = \sqrt{(x - x_{ic})^2 + (y - y_{ic})^2} \tag{4}$$

After k iterations, the model corresponding to the maximum number of inliers is selected. The circle center coordinates obtained from this optimal iteration are taken as the final solution for the cross-sectional center.

2.1.2 Solution for Threshold [d]

The threshold [d] is the criterion used in the RANSAC algorithm to distinguish inliers from outliers, and its selection is therefore critical. For wooden columns in traditional timber buildings, the cutting depth and surface irregularity largely determine the appropriate magnitude of [d]. However, these characteristics

are difficult to directly measure and quantify in practical surveys. In addition, instrumental and human operational errors can also introduce spurious "outliers." In theory, the error of the estimated center coordinates could be derived using error propagation formulas, but such derivations are highly complex. Moreover, there is a lack of published statistical analyses addressing measurement errors specifically in the surveying and mapping of ancient architectural structures. Consequently, determining a suitable and robust threshold remains a practical challenge.

In this study, an adaptive RANSAC algorithm is adopted to determine the threshold [d]. The term adaptive refers to a data-driven strategy for selecting [d], which is a core parameter of the RANSAC procedure. By incorporating the fundamental error characteristics of total station measurements, the proposed approach dynamically adjusts the threshold for round wooden columns with different diameters through statistical iterative analysis, thereby overcoming the limitations of empirical threshold selection in conventional RANSAC applications. The detailed procedure is as follows. First, a Monte Carlo random sampling simulation [25] is conducted to statistically analyze the error of the fitted circle center. The mean deviation of the circle center under the maximum allowable measurement-point error is taken as the initial value of the threshold [d]. Next, the threshold [d] is varied within a range of three times the standard deviation (3σ) to obtain the distribution characteristics of the inlier ratio w. Finally, the convergence behavior of the inlier proportion w is examined through repeated iterations to determine the optimal value of [d]. For a typical total station, the horizontal measurement accuracy is ±(2 mm + 2 ppm) [26]. Because the incremental error associated with long-distance measurement is relatively small in practical applications, it is neglected in this study, and 2 mm is adopted as the acceptable maximum error for measurement points P_1~P_3. This value is also regarded as the maximum permissible error for non-abnormal points (inliers) and is used in subsequent iterative calculations. It is assumed that the proportion of inliers among all measured points is w, and the number of iterations is set to 10,000. The final threshold [d] is obtained by continuously adjusting [d] and analyzing the relationship between [d] and w.

MATLAB R2016 was used for numerical simulation and testing. To mimic the actual distribution of measurement points on damaged or cut column surfaces, random points deviating from an ideal circular profile were generated based on a standard circle, including both inliers and outliers. Using cross-sections with different diameters as simulation objects, 10,000 measurement points were generated for each section, and 500, 1000, 2000, and 3000 outliers were added, corresponding to inlier ratios of 95%–70% (i.e., outlier proportions of 5%–30%). The distance deviations of outliers were set to 2–5 mm, 10, 15, and 20 mm, respectively, whereas the deviations of inliers were constrained within 0–2 mm. During the computation, the threshold [d] was increased incrementally in an arithmetic sequence starting from an initial value of 2 mm. In this way, the variation characteristics of the inlier proportion w for circular sections with different diameters under total station measurement conditions were obtained, providing a basis for rational determination of the threshold [d].

To verify whether the RANSAC algorithm with the selected threshold [d] can effectively remove outliers, a validation experiment was conducted. For each circular cross-section, 10,000 measurement points were first generated. Random outliers with distance deviations of 2–20 mm were then introduced, accounting for 5%, 10%, 20%, and 30% of the total points, respectively. The RANSAC algorithm using the determined threshold [d] was applied to estimate the circle center coordinates and radius. For comparison, the traditional LSM was also used to fit the circle center using the same datasets containing outliers.

2.1.3 Optimization of Measuring Point Layout

The threshold [d] discussed above was determined using a large-sample dataset of up to 10,000 measurement points. This sample size ensures that the statistical relationship between [d] and the inlier

proportion w is robust and that the inherent variation trends are clearly observable. However, in practical field measurements, the number of available points is often much smaller due to various constraints. In addition, wooden columns are frequently located adjacent to walls, or certain areas may be inaccessible because of preservation requirements in traditional timber buildings, as illustrated in Fig. 2. These limitations make it difficult to arrange measurement points around the full 360° circumference of the column, and in practice only three-quarters (270°) or even a semicircle (180°) may be measurable. A very small number of points also complicates the identification and removal of outliers, while a narrow angular range between points reduces the distance between adjacent points, impairing both operational feasibility and measurement accuracy. Consequently, it is necessary to investigate the optimal number of measurement points for different angular coverage ranges on the circular cross-section.

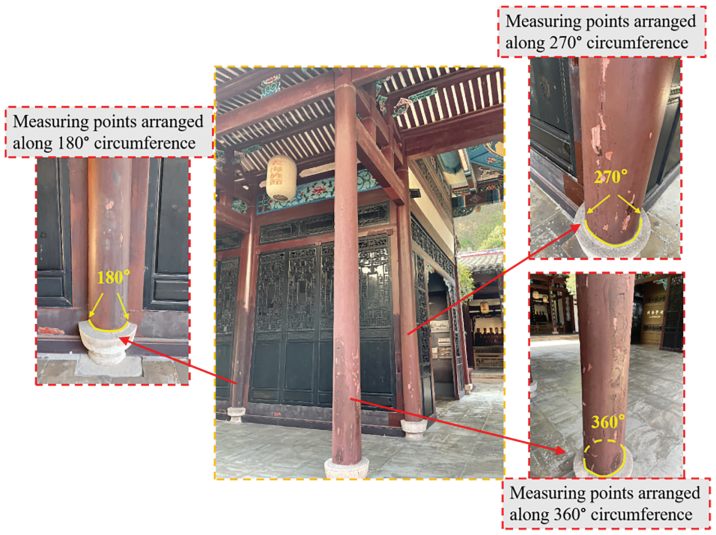

Figure 2: Angular ranges for arranging timber column inclination measuring points (180°, 270°, 360°).

MATLAB was used to simulate and analyze how measurement errors vary with the number of measurement points. Based on field investigations, 10 to 24 points were evenly distributed along 180°, 270°, and 360° circumferences of the column cross-section. Among these points, 0 to 5 outliers with errors ranging from 2 to 20 mm were introduced, with the maximum outlier proportion limited to 25%. The maximum error for non-outlier points was set to 2 mm, corresponding to the allowable error of the measuring instrument. After 10,000 iterative simulations, the statistical distribution of errors between the computed circle center coordinates and the standard origin (0, 0) was obtained at a 95% confidence level. The relationships between these errors, the number of measuring points, and the outlier proportion were then analyzed to determine the optimal number of measurement points for practical applications.

2.2 Calculation of Inclination Direction Vector of Wooden Columns Based on PCA

As described above, the RANSAC algorithm is first used to fit the center coordinates of circular wooden columns at different cross-sectional heights, accounting for defects and cut surfaces. Subsequently, PCA is applied to reduce the dimensionality of these high-dimensional spatial coordinates, fitting them to a low-dimensional straight line [27,28]. The inclination of the wooden column is then determined by calculating the direction vector of the axis defined by the line connecting the centers of all cross-sections.

2.2.1 Fitting of Axis Direction Vector of Circular Timber Column

The spatial coordinates of the center points are first centralized, and the covariance matrix is then computed, as expressed in Eqs. (5) and (6).

$$\boldsymbol{X}_{\text{centered}} = \boldsymbol{X} - \overline{\boldsymbol{X}} \tag{5}$$

$$C = \frac{1}{M-1}\boldsymbol{X}_{\text{centered}}^{\text{T}}\boldsymbol{X}_{\text{centered}} \tag{6}$$

The eigenvalues and eigenvectors of the covariance matrix C are calculated, where each eigenvalue $\boldsymbol{\lambda}_i$ and its corresponding eigenvector $\boldsymbol{v}_i$ satisfy Eq. (7). The eigenvalue $\boldsymbol{\lambda}_i$ represents the magnitude of variance of the data along a specific direction, while the eigenvector $\boldsymbol{v}_i$ indicates that corresponding direction in space.

$$\boldsymbol{C}\boldsymbol{v}_i = \boldsymbol{\lambda}_i\boldsymbol{v}_i \tag{7}$$

The maximum eigenvalue $\boldsymbol{\lambda}_{\max}$ is extracted from the set of all eigenvalues, along with its corresponding eigenvector $\boldsymbol{v}_{\max}$. This eigenvector $\boldsymbol{v}_{\max}$ indicates the principal direction of the data distribution, representing the linear trend fitted through the spatial coordinates of all points. The resulting straight line passes through the data center and is oriented along $\boldsymbol{v}_{\max}$. Its parametric equation can be expressed as shown in Eq. (8).

$$r(t) = \overline{x} + t\boldsymbol{v}_{\max} \tag{8}$$

where, t is a parameter representing displacement along the direction of the straight line. Specifically, if $\boldsymbol{v}_{\max} = [\,\boldsymbol{v}_x, \boldsymbol{v}_y, \boldsymbol{v}_z]^{\text{T}}$, the linear equation of the inclination vector of the circular wooden column can be expanded as shown in Eq. (9).

$$\begin{cases} x = \overline{x} + t\boldsymbol{v}_x \\ y = \overline{y} + t\boldsymbol{v}_y \\ z = \overline{z} + t\boldsymbol{v}_z \end{cases} \tag{9}$$

2.2.2 Number of Section Divisions

The accuracy of the PCA algorithm in determining the axis direction vector from multiple center points is directly influenced by the number of points used. Therefore, it is essential to investigate the number of cross-sections selected for wooden columns in field measurements (i.e., the number of corresponding circle center coordinates). This section focuses on two main aspects. First, while ensuring that the calculated circle center coordinates of cross-sections at different heights meet the required accuracy, the performance of the PCA algorithm itself in determining the axis direction of cylindrical columns is evaluated. Second, based on the minimum reasonable number of measurement points per cross-section, the minimum number of cross-sections required for wooden columns to satisfy engineering measurement accuracy standards is determined.

MATLAB was used to perform numerical simulations to investigate the two aspects described above. Using a lifted-beam timber frame system [29] as the research model and referring to relevant specifications and literature, the vertical columns were assigned an aspect ratio (height-to-base diameter) of 10:1 and a vertical taper of 1/100. Several equally spaced measuring cross-sections were defined along the height of the wooden column, with 10,000 measurement points arranged per cross-section and an outlier proportion of 10%, ensuring that the calculated circle center coordinates met the required accuracy standards. The allowable inclination limit, $\Delta = H/250$ specified for traditional timber frames in the Chinese Specification [1], was adopted as the target threshold to verify the accuracy of the axis direction vector obtained via the

PCA algorithm. Subsequently, the minimum reasonable number of measurement points per circular cross-section, as determined in Section 2.1.3, was applied to the algorithm for 10,000 iterative calculations. From these simulations, the relationship between the measured column inclination and the number of cross-section divisions was established at a 95% confidence level, thereby determining the optimal number of cross-section divisions for wooden columns of varying heights.

2.3 Field Measurement

Field tests were conducted on a Qing Dynasty ancestral hall in China [30], as shown in Fig. 3. Three wooden columns, labeled L1–L3, located at the center of the hall, were selected for inclination measurement. Field investigation revealed that one-quarter of the circumference of column L1 was attached to an adjacent wall, whereas columns L2 and L3 were free-standing. The diameters of the three columns ranged from 300 to 350 mm, with heights between approximately 5 and 6 m. Inspection of the columns' in-service condition indicated partial paint peeling at the base of all three columns, with similar peeling also observed at the mid-height of column L3. Additionally, cutting surfaces were present at the bases of columns L1 and L2, accounting for roughly one-eighth of the total circumference of each column.

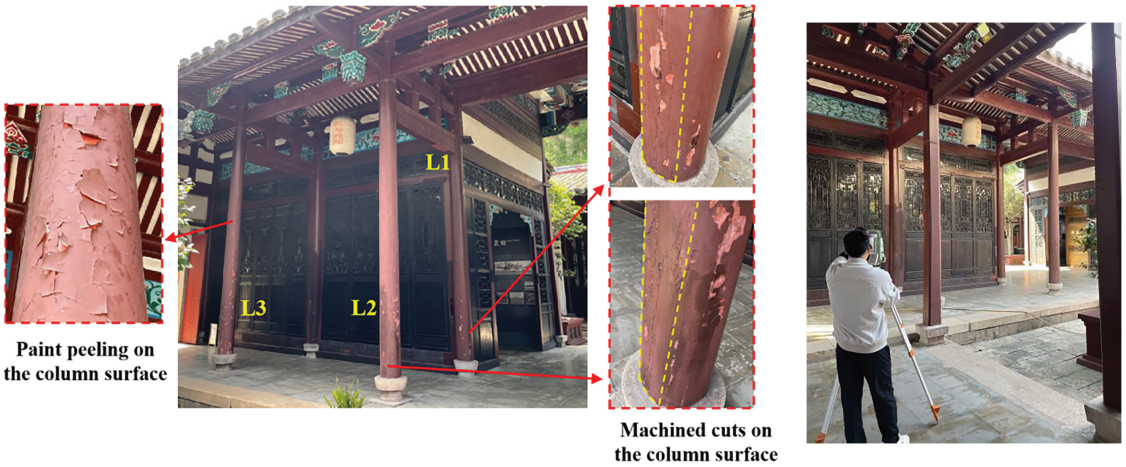

(**a**) Field investigations on in-service status of wooden columns (**b**) Field test

Figure 3: Field measurement of a traditional timber ancestral hall of Qing Dynasty in China.

A total station was used to measure the 3D spatial coordinates of the column surfaces, and the inclinations of the three wooden columns were calculated using the proposed method based on the adaptive RANSAC and PCA algorithms. Simultaneously, a 3D laser scanner was employed to capture dense point cloud data from the surfaces of the three cylindrical columns. The scanner's built-in software was then used to perform conical surface fitting on the point cloud data, yielding the central axis vector of each column for comparison with the results obtained using the proposed method. For column L1, however, one-quarter of the circumference was obstructed by a wall, rendering that portion inaccessible for scanning. As a result, the axial inclination vector of L1 could not be directly obtained via the scanner's built-in cone-fitting procedure. Instead, the defect-free top and bottom cross-sections of L1 were selected, and the circle centers were fitted using the LSM to determine the column's inclination vector.

3 Results

3.1 Simulation Results

3.1.1 Threshold [d] Determination Results

Taking a cross-section with a diameter of D = 400 mm as a case study, the variation curve of the inlier proportion w was obtained, as shown in Fig. 4. In the figure, the legend "10%/2–5" indicates that 10% of the points (i.e., 1000 out of 10,000) were designated as outliers, corresponding to an inlier proportion w of 90%, with outlier errors ranging from 2 to 5 mm. As shown in the curve, in the initial phase, the inlier proportion $w$increases linearly with the threshold [d], and the inliers are relatively uniformly distributed, indicating a strong linear correlation between [d] and w. As [d] increases further, the growth rate of w gradually slows, suggesting that the number of inliers approaches the true value (red dashed line in Fig. 4). In practical field measurements, the true inlier proportion w is unknown. However, Fig. 4 demonstrates that for true inlier proportions ranging from 70% to 95% (i.e., 5%–30% outliers), the threshold [d] at the proportional limit point of the w curve lies approximately between 1.9 and 2.4 mm, with minimal fluctuation. Based on these adjustments, a mean value of [d] = 2.2 mm was adopted as the general threshold for the D = 400 mm cross-section. Table 1 summarizes the final threshold values for circular cross-sections of different diameters.

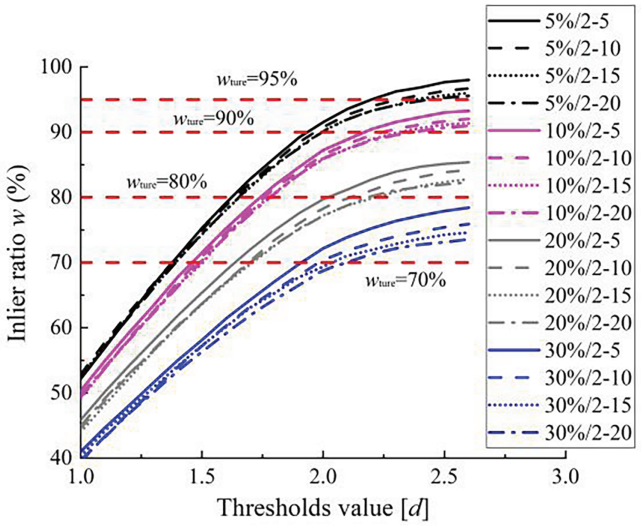

Figure 4: Curve of relationship between inlier ratio and the threshold value [d] for wooden column with diameter D = 400 mm.

Table 1: Values of Threshold [d] for different diameters of measured wooden column.

Diameter of wooden column cross-section D	200 mm	400 mm	600 mm	800 mm	1000 mm
Threshold for RANSAC algorithm [d]	2.1 mm	2.2 mm	2.4 mm	2.6 mm	2.8 mm

The verification results for circle center coordinate accuracy using the threshold values [d] recommended in Table 1 are presented in Fig. 5. Due to space limitations, only the results for the cross-section with D = 200 mm are shown. Fig. 5 illustrates the fitted circle center coordinates (denoted as OR) and radius (R) under varying outlier proportions. For comparison, the circle center coordinates obtained using the traditional LSM, denoted as OL, are also displayed. As observed, increasing the proportion of outliers

had little effect on the coordinates OR or the radius R; the maximum deviation of O_R from the standard center (0.00, 0.00) was only approximately 0.1 mm. In contrast, the deviation of OL increased progressively with higher outlier proportions. When the outlier proportion reached 30%, the deviations of OL from the standard center along the *X*- and *Y*-axes were 1.25 and 1.55 mm, respectively. These results demonstrate that the RANSAC algorithm, combined with the threshold [*d*] values in Table 1, effectively eliminates random outliers, significantly improving the accuracy of circle center determination compared with LSM. Verification tests for other cross-sections with different diameters yielded consistent results, which are not presented here due to space constraints.

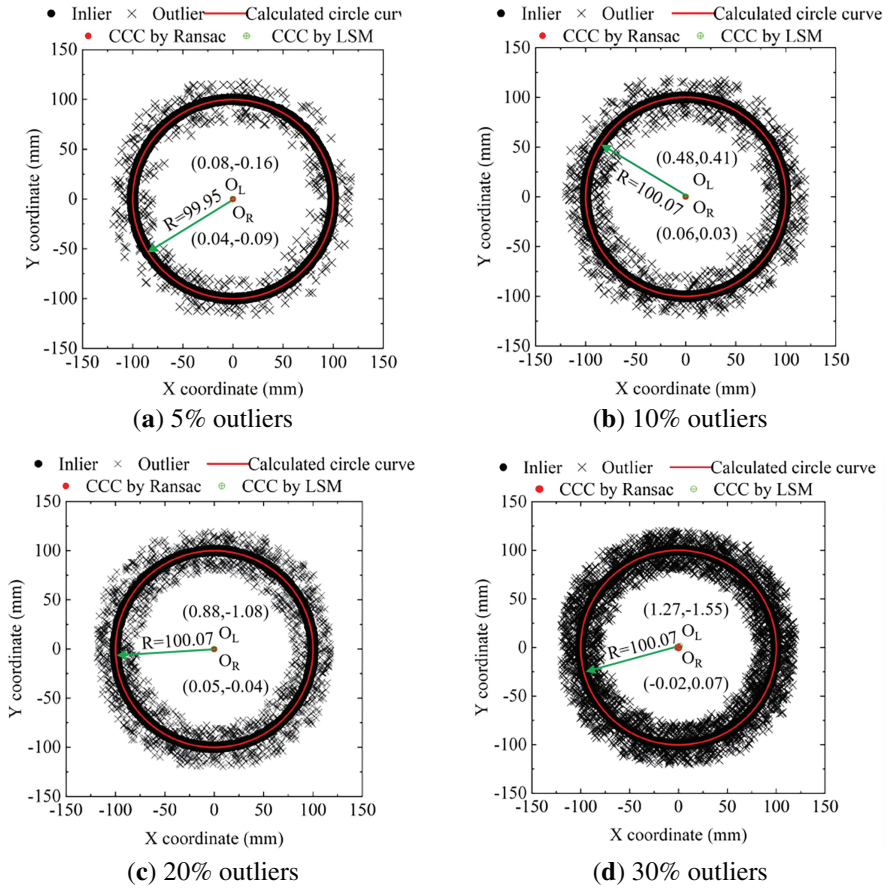

(**a**) 5% outliers (**b**) 10% outliers

(**c**) 20% outliers (**d**) 30% outliers

Figure 5: Simulation results of the circular cross-section with diameter *D* = 200 mm under different outlier proportions.

3.1.2 Influence of Measuring Points and Layout Ranges

The statistical results of the errors between the calculated circle center coordinates and the standard origin (0, 0) at a 95% confidence level are presented in Fig. 6. Due to space limitations, only the results for the circle with *DD* = 400 mm are shown, where panels (a)–(c) correspond to measuring points uniformly distributed over 360°, 270°, and 180° ranges, respectively. As observed, the circle center calculation error decreases as the number of measurement points increases and increases with the number of outliers. When the number of outliers exceeds a certain threshold, the error growth rate rises sharply. For the same number of measurement points and outliers, reducing the angular range of point arrangement leads to larger errors. In particular, when the measurement range is limited to 180°, the center error remains higher than the instrument error (2 mm) even when the number of measurement points is increased to 24.

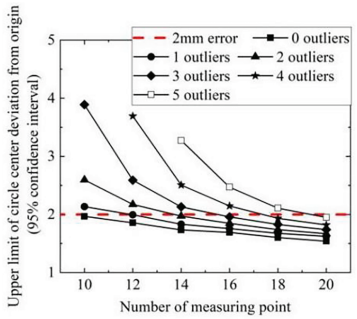

(**a**) Measuring points arranged along the full 360° circumference

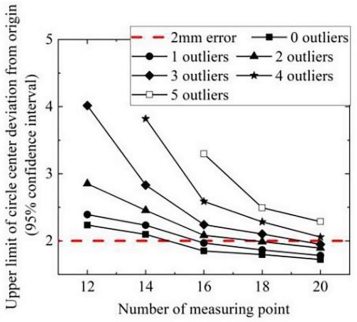

(**b**) Measuring points arranged along the 270° three-quarter circumference

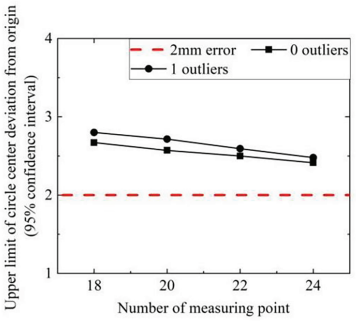

(**c**) Measuring points arranged along the 180° semicircular circumference

Figure 6: Upper limit of the calculation error of the center coordinates for 400 mm-diameter circular cross-section under different measuring points numbers (95% confidence interval).

Using the 2 mm error upper limit at a 95% confidence level (corresponding to the red dashed line in Fig. 4) as the critical criterion, Table 2 summarizes the maximum allowable number of outliers for different numbers of measurement points and layout angle ranges for wooden columns of various diameters. In Table 2, "***n***" represents the number of outliers, "***N***" denotes the minimum number of measurement points required, and the layout angle range is restricted to θ = 270°~360°. For a uniform measurement point layout, the outlier proportion approximately corresponds to the ratio of the arc length of damaged or defective regions on the column surface to the total circumference of the column.

Table 2: Minimum measuring points number N where calculation error does not exceed instrument error.

	Layout Range *θ*		
***n*: Outlier No.**	***N* (360°)**	***N* (270°)**	***N* (180°)**
0	14/12/12/12	16/16/16/14	/
1	14/14/12/12	16/16/16/16	
2	16/16/14/14	18/18/16/16	
3	16/16/16/16	20/20/20/20	
4	18/18/18/18	/	
5	20/20/20/20	/	

Note: The table values correspond to wooden columns with diameters *D* = 200/400/600/800 mm in sequence.

3.1.3 Influence of Cross-Section Number

A tapered round wooden column with a height of 5 m and a taper ratio of 1/100 was selected as the research object. Three to six equally spaced cross-sections were defined along the column, and 10,000 randomly sampled measurement points (with an outlier ratio of 10%) were generated for each cross-section. The tilt angles of the wooden column calculated using the PCA algorithm are presented in Fig. 7. In the figure, the red dashed line represents the target inclination vector corresponding to $\Delta = H/250$ specified in Chinese standards [1], the green solid line denotes the calculated axis direction vector of the wooden column, and $\boldsymbol{\alpha}$ represents the angle between the column's axis and the ground plane. The results indicate that the column's axis direction vector closely aligns with the target inclination vector of $\Delta = H/250$. Specifically, the angle between the wooden column axis and the geodetic normal ranges from 89.769° to 89.770°, corresponding to a tilt angle of 0.230°–0.231°. The equivalent tilt displacement is $\Delta = H/248.7$ to $H/247.7$, with a maximum deviation of only 1.2% from the theoretical value of $H/250$. These results demonstrate that, with a sufficient number of measurement points, the proposed method can accurately determine the inclination of wooden columns while effectively accounting for outliers.

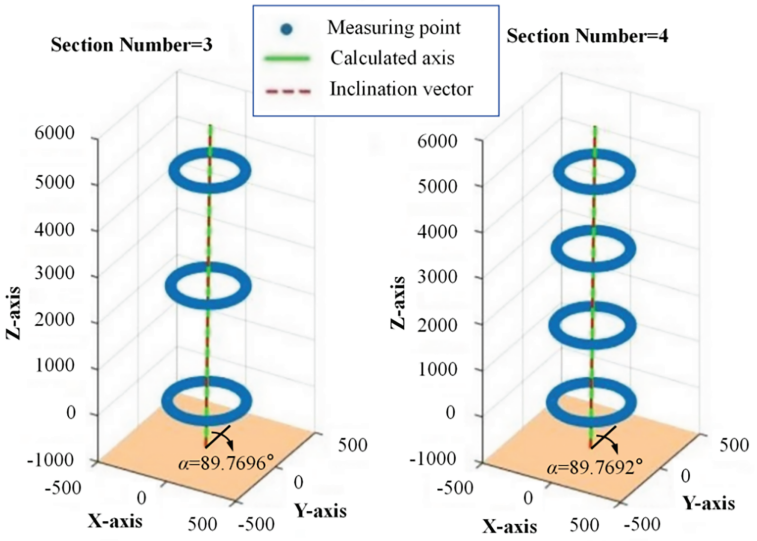

(**a**) Calculation results when the number of cross-sections = 3 and 4

Figure 7: (Continued)

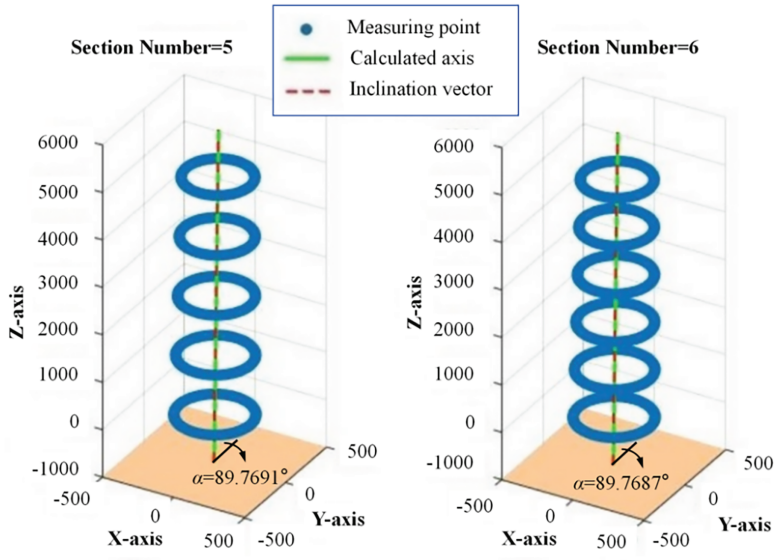

(**b**) Calculation results when the number of cross-sections = 5 and 6

Figure 7: Calculation results of axis inclination for circular wooden columns when the number of measuring points N = 10,000.

Considering the actual field measurement conditions, the number of measuring points for each circular cross-section was selected according to the recommended minimum configuration listed in Table 3. Using $\Delta = H/250$ (corresponding to a tilt angle of 0.0040 rad) as the control target, 10,000 repeated simulations were conducted in MATLAB. The calculated upper limits of the inclination angles of round wooden columns at a 95% confidence level are summarized in Fig. 8. Here, the values are defined as the upper limit of the inclination ($\mu + 2\sigma$) and represent the statistically derived results of column inclination in this study. The results indicate that, as the number of cross-sections increases, the calculated inclination values gradually converge toward 0.0040 rad. Calculation accuracy also improves with increasing column height. Using a 7% relative error as the classification criterion, the minimum number of cross-section divisions required for accurate tilt measurement of traditional wooden columns is summarized in Table 3.

Table 3: Minimum section number for inclination measurement at different heights of column (7% error limit).

Height of column H	5 m	6 m	7 m	8 m	9 m	10 m
Section number (360° range measurement)	6	5	5	5	5	5
Section number (270° range measurement)	6	5	5	5	5	5

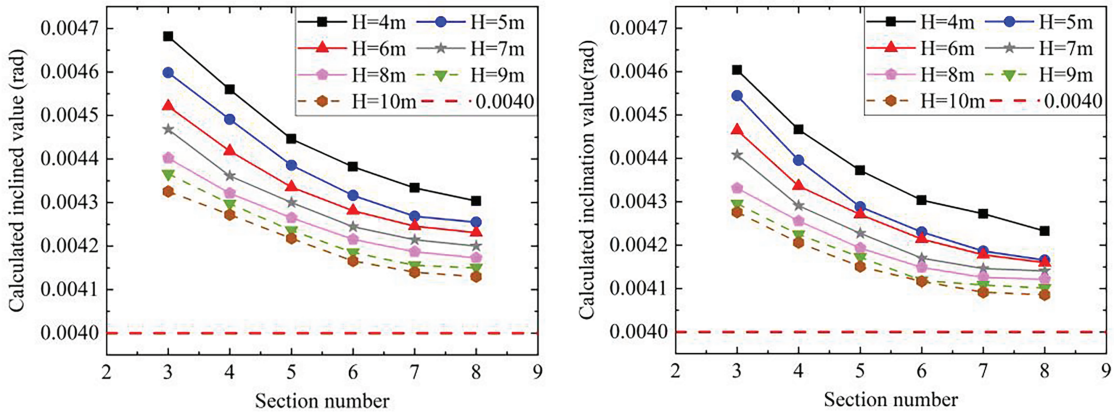

(**a**) 270° range measurement in cross-section (**b**) 360° full cross-section measurement

Figure 8: Upper limit of inclination calculation for circular wooden columns with a 95% guarantee rate.

3.2 Field Validation Results

Fig. 9 illustrates the inclination measurement results of columns L1–L3 obtained using the adaptive RANSAC algorithm combined with PCA. The figure shows the circle centers of each cross-section, the calculated inclination vectors, and the angles between these vectors and the ground plane, both in 3D space (with the *X* and *Y* axes corresponding to the ground plane and the *Z* axis representing column height) and projected onto the *X*–*Y* plane. Points a1–a3 and b1–b3 denote the intersections of the calculated inclination vectors with the bottom and top section planes of the columns, respectively. Measurement points identified as outliers by MATLAB are marked with green "×" symbols.

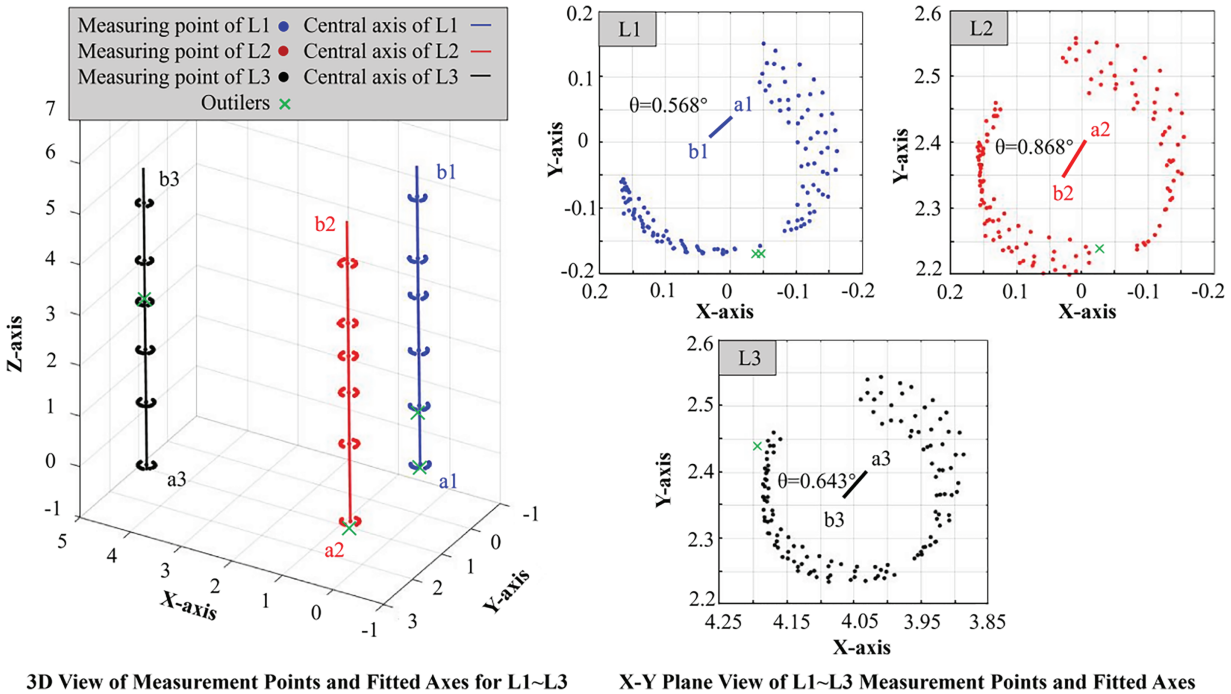

3D View of Measurement Points and Fitted Axes for L1~L3 **X-Y Plane View of L1~L3 Measurement Points and Fitted Axes**

Figure 9: Inclination measurement results of traditional timber columns L1-L3 based on adaptive RANSAC and PCA.

Fig. 10 presents the results obtained from 3D laser point cloud scanning. It shows the point clouds of columns L1–L3, the fitted central axis vectors, and the angles between these vectors and the X–Y ground plane in both 3D space and the X–Y plane. Here, A1–A3 and B1–B3 represent the intersections of the fitted central axes with the bottom and top section planes, respectively.

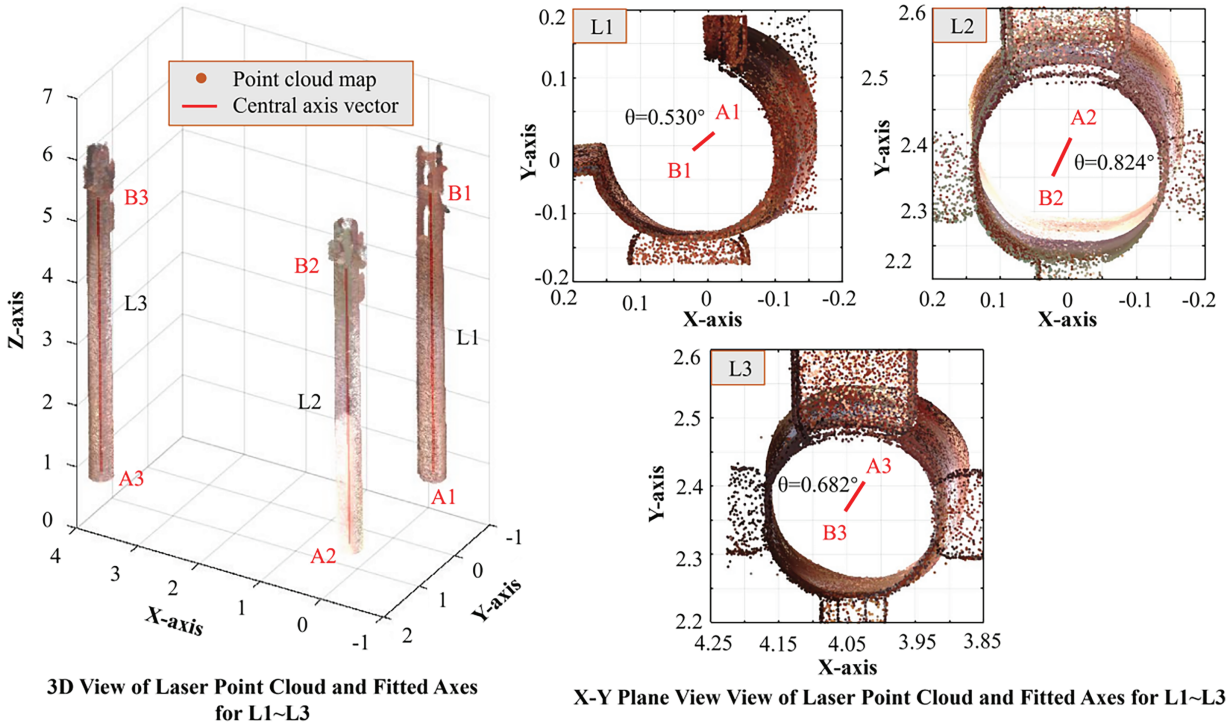

Figure 10: Inclination measurement results of wooden columns L1-L3 based on 3D scanning technology.

Comparison of Figs. 9 and 10 indicates that the inclination vectors obtained by the proposed method closely match those derived from 3D point clouds. The inclination directions in the X–Y plane are fully consistent, pointing from the coordinate origin toward the positive X- and Y-axis directions. Moreover, the angles between the inclination vectors and the ground plane (Z-axis) calculated by the two methods are in close agreement. Specifically, for column L1 (with a 270° measurement point layout), the calculated inclination angle in Fig. 9 is 0.568°, compared with 0.530° from 3D laser scanning in Fig. 10. For columns L2 and L3 (both with 270° layouts), the inclination angles calculated using the proposed method are 0.868° and 0.643°, respectively, vs. 0.824° and 0.682° obtained from 3D laser scanning, corresponding to relative errors below 7%. In addition, Fig. 9 highlights the measurement points identified as outliers by the adaptive RANSAC algorithm, marked with green "×" symbols. These outliers are located at the bases of columns L1 and L2 and at the mid-height of column L3, aligning with the expected defective regions.

4 Discussion

4.1 Determination and Rationality Analysis of Threshold [d]

Fig. 3 illustrates the relationship between the calculated inlier ratio and the threshold [d] in the RANSAC algorithm. In the initial ascending phase of the curve, the inlier ratio increases approximately linearly with the threshold [d]. Once the curve exceeds the proportional limit, the growth of the inlier ratio becomes more gradual, indicating that the algorithm's ability to eliminate outliers diminishes and it becomes

difficult to accurately identify inliers. An excessively small [d] may erroneously exclude valid measurement points, whereas an excessively large [d] fails to effectively remove outliers. As shown in Fig. 3, near the proportional limit point, the calculated inlier ratio closely approximates its true value. Therefore, the [d] value corresponding to the proportional limit is selected as the final threshold in this study.

Analysis of the curve characteristics under varying outlier ratios and dispersion levels indicates that the threshold [d] values determined by this method consistently fall within the range of 1.9–2.3 mm, showing minimal fluctuation. This confirms both the stability and rationality of the proposed threshold and effectively eliminates the subjective bias associated with manually setting the threshold. It should be noted that the threshold determination method described above is based on the accuracy specification of ±(2 mm + 2 ppm) for commonly used total stations. If a total station with a lower accuracy is employed in field measurements, it is necessary to recalculate the correlation curve between the threshold and the inlier ratio and determine the appropriate threshold [d] using the adaptive approach outlined in Section 3.1.3.

4.2 Rationality and Application Analysis of the Number of Measurement Points

Fig. 5 illustrates the relationship between the number of measurement points and the calculation error of circle center coordinates. Notably, when measurement points are distributed only within a 180° range (i.e., a semicircle) of the circumference, even 24 points fail to satisfy the accuracy requirements. Further increasing the number of points yields only limited improvement, while excessively dense layouts can reduce both operational feasibility and measurement accuracy. Therefore, the proposed method is not suitable for wooden columns with a measurable range restricted to 180°.

The procedure for applying the data in Table 2 to field measurements is as follows. First, inspect the column surface to estimate the proportion of defective areas under a uniform measurement point arrangement. Then, determine the minimum required number of measurement points with reference to Table 2. For example, consider a wooden column cross-section with a diameter of D = 400 mm. Suppose the estimated damaged area accounts for 10% of the circumference, and wall obstructions limit the measurement range to 270°. According to the data in the fourth row and third column of Table 2, with 16 measurement points (N = 16), the maximum allowable number of outliers is n = 2, corresponding to an outlier proportion of 2/16 = 12.5%. Since this exceeds the estimated 10% damage ratio, the configuration satisfies the error control requirements. Therefore, a minimum of 16 measurement points is required to ensure that the circle center error does not exceed the instrument error at the 95% confidence level.

Further analysis of Table 2 reveals the following: when measurement points are arranged along a 270° circumference, the maximum allowable number of outliers for 16 points is four; when there is no wall obstruction and points can be arranged along a full 360° circumference, the maximum allowable number of outliers for 20 points is five. In both cases, the outlier ratio is 25%. Considering that increasing the number of measurement points would result in an excessively dense layout and substantially increase field workload, this study concludes that, in practical application, the proportion of defective areas on the cross-section of a wooden structural column should not exceed 25% of the total circumference. Otherwise, the RANSAC algorithm may fail to meet the preset error control requirements. Due to the practical difficulty of field measurement in such scenarios, these cases are not included in Table 2. Moreover, the above measurement point layout assumes that the cross-section is circular and that points are uniformly distributed along the circumference. These assumptions are well-supported in practical engineering contexts: the cross-sectional profiles of traditional timber columns are predominantly circular or square, and field operators can achieve uniform division of measurement points prior to data acquisition.

4.3 Rationality and Optimization Analysis of the Number of Cross-Section Divisions

Fig. 7 shows the correlation between the calculated tilt values of timber columns and the number of cross-section divisions, with the control target set as $\Delta = H/250$ (corresponding to a tilt angle of 0.0040 rad). As shown, the calculated tilt values gradually converge toward the true values as the number of section divisions increases. Additionally, for a given number of divisions, taller timber columns exhibit higher tilt calculation accuracy. This is because the instrument error is strictly controlled within 2 mm in this study. As the size of the measured component increases, the relative impact of this fixed error on the overall tilt calculation diminishes, producing the observed trend that "the taller the column, the higher the calculation accuracy." Notably, for timber columns shorter than 5 m, the small component size amplifies the influence of instrument error. Even with a substantial increase in the number of cross-section divisions, achieving the precision required for engineering measurement remains challenging. Therefore, the proposed method is not recommended for inclination detection of short timber columns.

4.4 Comparative Verification and Advantage Analysis of the Proposed Method

Figs. 9 and 10 present the inclination measurement results of the wooden columns obtained using the proposed method and 3D laser scanning technology, respectively. Comparing Fig. 9 with the field investigation results (Fig. 4), the positions of the identified outliers (marked with green "×") show a high degree of agreement with the observed defects. Specifically, the cutting surface defects at the bases of columns L1 and L2, as well as the paint peeling observed at mid-height of column L3, correspond precisely with the abnormal measurement points identified in Fig. 9. This confirms that the proposed method effectively identifies and eliminates outlier points caused by inherent defects in wooden columns, providing a reliable basis for accurate inclination calculation.

It is important to note that, in field measurements, neither the proposed method nor 3D laser scanning can directly obtain the true tilt angle of ancient timber columns. The results from both approaches are approximations derived from fitting or iterative algorithms. This contrasts with numerical simulations, where the target tilt value is predetermined. Consequently, the accuracy of the proposed method can only be evaluated against well-established measurement technologies in practice. 3D laser scanning was chosen for comparative verification for two main reasons: (1) it provides extremely high measurement accuracy, serving as a reliable benchmark in engineering detection, and (2) it rapidly acquires dense point cloud data on the column surface, which, when used with traditional fitting methods, effectively mitigates the influence of small-scale surface defects on overall fitting accuracy. Therefore, the cylindrical surface fitting approach based on 3D laser point clouds can be considered a reliable reference for the true inclination of wooden columns.

Furthermore, comparison of the results in Figs. 9 and 10 shows that the inclination vectors and tilt angles obtained using the proposed method are highly consistent with those derived from 3D laser cylinder fitting. The proposed method also demonstrates significant technical and economic advantages. It requires considerably fewer measurement points, can rapidly output results through MATLAB programming, and is far more computationally efficient than processing and segmenting over 10,000 laser-scanned points. Additionally, only a total station and a standard computer are needed for measurement and analysis, reducing both equipment purchase and operational costs compared with 3D laser scanning and high-performance computing requirements.

Overall, the proposed method offers clear advantages for field monitoring scenarios where only a total station and an ordinary computer are available. It can reliably measure the inclination of ancient timber columns with defects, demonstrating strong engineering practicality and adaptability to various measurement conditions.

4.5 On-Site Engineering Operation Procedure and Application Instructions

This section outlines the on-site engineering application procedure for the proposed method, serving as a direct reference for measurement personnel. All iterative calculations can be efficiently performed using MATLAB, ensuring convenient operation and high computational efficiency. The specific steps are as follows:

(1) On-Site Investigation: Assess the measurement environment and conditions. Record key information including the height H and diameter D of the column, the extent of surrounding wall obstructions, the degree of surface damage, presence of artificial cuts, and on-site lighting and visibility conditions.
(2) Feasibility Analysis: The method is deemed inapplicable if any of the following conditions are met: the column height is less than 5 m, the effective measurement angular range is less than 270°, or the damaged area of the column surface exceeds 25% of the total cross-section.
(3) Measurement Preparation: Position transfer stations according to the site environment and the column location. Complete total station setup, calibration, and debugging. Determine the number of cross-sections N along the column height and the number of measurement points n per cross-section based on the guidelines provided in Tables 2 and 3.
(4) Measurement Point Acquisition: Using a total station, acquire 3D coordinates of measurement points evenly distributed along the circumference of each cross-section. If transfer stations are used, unify all data into a single coordinate system through appropriate transformations. Follow total station operating procedures strictly to ensure measurement accuracy.
(5) Iterative Analysis: Determine the RANSAC threshold $[d]$ with reference to Table 1. For each cross-section, randomly select three points to perform a single iteration according to Eqs. (1)–(4), and calculate the distance (d_i) from each remaining point to the fitted circle as well as the circle center coordinates. Repeat this process for 10,000 iterations. Points with $d_i > [d]$ are classified as outliers, while points with $d_i > [d]$ are considered inliers.
(6) Circle Center Determination: Identify the iteration with the maximum number of inliers. The circle center coordinates obtained in this iteration are adopted as the final coordinates for the cross-section.
(7) Axial Vector Calculation: Sequentially determine the circle centers of all cross-sections along the column height. Substitute these coordinates into Eqs. (5)–(9) to derive the spatial axis vector passing through all circle centers.
(8) Inclination Safety Assessment: Calculate the angle between the column's axial vector and the horizontal plane of the earth to obtain the actual inclination. Compare this angle with the allowable limit (H/250) to assess whether the column's inclination exceeds the permissible range.

5 Conclusions

This study proposed a method for calculating the inclination of wooden columns based on the adaptive RANSAC algorithm and PCA. The influences of column cut surfaces, defects, the number of measuring points, the number of cross-sections, and the layout positions of measuring points on calculation accuracy were systematically investigated. The main conclusions are summarized as follows:

(1) Adaptive RANSAC for Cross-Section Center Calculation: A solution based on the adaptive RANSAC algorithm was developed to determine the centers of cross-sections in traditional timber columns. Statistical analyses clarified the effects of the number of measuring points, their layout positions, and the proportion of outliers on calculation accuracy. Recommended values for the outlier discrimination threshold, the number of measuring points, and their layout positions are provided.
(2) Inclination Measurement via PCA and RANSAC Integration: An indirect measurement approach for column inclination was established by integrating PCA with the adaptive RANSAC algorithm. Using

statistical analysis, recommended values for the number of cross-section divisions for columns of varying heights were determined, providing practical parameter references for field application.

(3) Field Verification: Field tests were conducted in a Qing Dynasty ancestral hall. The results demonstrated that the proposed method effectively identifies and eliminates outlier points caused by cut surfaces and defects. Compared with 3D laser scanning technology, which is costly and generates massive datasets, the proposed method achieves required measurement accuracy using only a limited number of points, highlighting its strong engineering practicality.

(4) Applicability and Limitations: The method is not recommended for columns with a measurable angular range of only 180° or when defective areas exceed 25% of the cross-sectional circumference. Future research could extend the approach to square wooden columns and optimize the algorithm for columns exhibiting severe deformation.

Acknowledgement: The authors would like to express their sincere gratitude to Houming Zhuang and Lubin Zhang from the research group for their valuable assistance in the field test section.

Funding Statement: These works were supported by Funding statement as follows: The Guiding (Key) Project Funding for Social Development in Fujian Province (2021J011063); Fujian Education and Research Project for Young and Middle-aged Teachers (Science and Technology category) (JAT220227); and Science and Technology Project of Fujian University of Technology (GY-Z220226).

Author Contributions: The authors confirm contribution to the paper as follows: Conceptualization, Minyan Zhan, Minghao Wu; methodology, Minyan Zhan, Wei Yang; software, Minyan Zhan; validation, Minghao Wu, Hsin-Yi Wang, Yu-Hsien Ho; formal analysis, Minyan Zhan, Minghao Wu; investigation, Minyan Zhan; resources, Wei Yang, Minghao Wu; data curation, Minghao Wu; writing, original draft preparation, Mingyan Zhan, Minghao Wu; writing, review and editing, Hsin-Yi Wang, Yu-Hsien Ho; visualization, Minghao Wu; supervision, Wei Yang; project administration, Minghao Wu; funding acquisition, Wei Yang. All authors reviewed and approved the final version of the manuscript.

Availability of Data and Materials: The data that support the findings of this study are available from the Corresponding Author, Minghao Wu, upon reasonable request.

Ethics Approval: Not applicable.

Conflicts of Interest: The authors declare no conflicts of interest.

References

1. GB/T 50165-2020. Technical standard for maintenance and strengthening of historic timber building. Beijing, China: China Architecture & Building Press; 2020. (In Chinese).
2. Qian C, Wang T, Yu S. Structural visualization analysis applied to the preservation of architectural heritage: the case of stilted houses in southwest Hubei. China Herit Sci. 2024;12(1):304. doi:10.1186/s40494-024-01420-0.
3. Shi X, Guo Z, Wang W, Li T, Chen J, Meng X. Effects of inclination on hysteretic behavior of asymmetric ancient timber structures. J Build Eng. 2025;116:114743. doi:10.1016/j.jobe.2025.114743.
4. Li NL, Jiang SF, Wu MH, Shen S, Zhang Y. Deformation monitoring for Chinese traditional timber buildings using fiber Bragg grating sensors. Sensors. 2018;18(6):1968. doi:10.3390/s18061968.
5. Jiang SF, Qiao ZH, Li NL, Luo JB, Shen S, Wu MH, et al. Structural health monitoring system based on FBG sensing technique for Chinese ancient timber buildings. Sensors. 2020;20(1):110. doi:10.3390/s20010110.
6. Fattore C, Porcari S, Priore A, Porcari VD. Non-invasive techniques for monitoring cultural heritage: change detection in dense point clouds at the San pietro barisano bell tower in matera. Italy Heritage. 2025;8(1):14. doi:10.3390/heritage8010014.
7. Liu S. Application of deformation detection method based on time-varying point cloud in the protection of ancient buildings. J Comput Meth Sci Eng. 2020;20(2):531–42. doi:10.3233/jcm-193902.

8. Wang L, Zhou JW, Wang HS, Jiang DP. Deformation monitoring of ancient towers based on 3D laser scanning technology. Bullet Surv Mapp. 2020;7(3/4):120–9. (In Chinese). doi:10.1504/ijiids.2025.10070972.
9. Guo M, Sun M, Pan D, Wang G, Zhou Y, Yan B, et al. High-precision deformation analysis of Yingxian wooden pagoda based on UAV image and terrestrial LiDAR point cloud. Herit Sci. 2023;11(1):1. doi:10.1186/s40494-022-00833-z.
10. Ortiz-Sanz J, Bastos G, Gil-Docampo M. Deformation measurement of twisted timber beam using UAV SfM photogrammetry and a new feature extraction algorithm. Eur J Wood Wood Prod. 2025;83(2):88. doi:10.1007/s00107-025-02245-9.
11. García-Nieto MC, Huesca-Tortosa JA, Martínez-Segura MA, Espín de Gea A, Navarro M. Structural deformation monitoring using UAV photogrammetry to assess slender historic buildings. J Build Eng. 2025;100:111766. doi:10.1016/j.jobe.2025.111766.
12. Zhou Y, Chen J, Hao G, Zhu S. Deformation monitoring of high-rise building clusters: acquiring deformation coefficients by combining satellite imagery and persistent scatterer interferometry. Struct Control Health Monit. 2024;2024(1):2326106. doi:10.1155/2024/2326106.
13. El-Ashmawy KLA. A simple methodology for monitoring and analysis of vertical displacement of buildings. Am Sci Res J Eng Technol Sci (ASRJETS). 2019;60(1):83–92.
14. Ma J, Liu D, Yan W, Liu G, Guo X. Crack detection and analysis method for timber structures of ancient buildings based on laser point cloud data. Meas Sci Technol. 2025;36(7):076010. doi:10.1088/1361-6501/ade3f7.
15. Wang XL, Jin L. Analysis of the influence of mortise-tenon joint damage on seismic performance of ancient timber structure. Appl Mech Mater. 2014;580-583:1595–9. doi:10.4028/www.scientific.net/amm.580-583.1595.
16. Wang X, Xu Q, Wang X, Guo J, Cao W, Xiao C. Strength degradation of wood members based on the correlation of natural and accelerated decay experiments. J Renew Mater. 2020;8(5):565–77. doi:10.32604/jrm.2020.09020.
17. Qin S, Yang N, Dai L. Rotational behavior of column footing joint and its effect on the dynamic characteristics of traditional Chinese timber structure. Shock Vib. 2018;2018(1):9726852. doi:10.1155/2018/9726852.
18. Ali Hassan Shah S, Shan J, Li P. UAV-based 3D segmentation and structural damage assessment of regional buildings. J Civ Struct Health Monit. 2025;15(8):4081–105. doi:10.1007/s13349-025-01030-9.
19. Min Y, Tang Y, Chen H, Zhang F. A linear fitting algorithm based on modified random sample consensus. Appl Sci. 2025;15(11):6370. doi:10.3390/app15116370.
20. Shen B, Buck D, Yuan Z, Zhu Z. Influencing factors of pine wood milling force based on principal component analysis and multiple linear regression. Materials. 2026;19(2):439. doi:10.3390/ma19020439.
21. Tarpø M, Ulriksen MD, Augustyn D, Dollerup N, Caglio L, Sørensen JD. Full-field stress estimation of offshore structures using modal expansion and principal component analysis. J Sound Vib. 2025;618:119295. doi:10.1016/j.jsv.2025.119295.
22. Dai J, Liu J, Yang J, Ran L, Xue F, He X. Correlational fractal analysis of the Kaiser effect in rock: implications for salt-cavern engineering under triaxial cyclic loading and unloading. Nondestruct Test Eval. 2025;40(3):1180–202. doi:10.1080/10589759.2024.2343943.
23. Kim Y, Yun S. Performance analysis of point cloud edge detection for architectural component recognition. Appl Sci. 2025;15(17):9593. doi:10.3390/app15179593.
24. Dal Poz AP, Yano Ywata MS. Adaptive random sample consensus approach for segmentation of building roof in airborne laser scanning point cloud. Int J Remote Sens. 2020;41(6):2047–61. doi:10.1080/01431161.2019.1683644.
25. Charmpis DC. The effect of correlations among random member properties on structural reliability. Structures. 2019;19(1):463–75. doi:10.1016/j.istruc.2019.02.002.
26. Qiu YX, Zhu J, Wang YH. Evaluation of uncertainty of distance measurement by total station using adaptive Monte Carlo method. Metrol Meas Technol. 2023;43(5):104–11. (In Chinese). doi:10.17814/mechanik.2017.12.195.
27. Jiang SF, Wu MH, Ma SL, Lin DY. Structural stiffness identification of traditional mortise-tenon joints based on statistical process control chart. J Aerosp Eng. 2018;31(5):04018066. doi:10.1061/(asce)as.1943-5525.0000894.
28. Zhang X, Otto F, Oeser M. Modeling pavement surface deflections under accelerated pavement testing using the PCA method. J Constr Eng Manage. 2021;147(12):04021169. doi:10.1061/(asce)co.1943-7862.0002203.

29. He JX, Yu P, Wang J, Yang QS, Han M, Xie LL. Theoretical model of bending moment for the penetrated mortise-tenon joint involving gaps in traditional timber structure. J Build Eng. 2021;42(1):103102. doi:10.1016/j.jobe.2021.103102.
30. Xiong W, Hu Z, Liu J, Ma K, Lu Z, Li X. Acoustic characteristics and influencing mechanisms of the traditional ancestral temple theatre in northeast Jiangxi. Heritage. 2025;8(12):515. doi:10.3390/heritage8120515.